IOP PUBLISHING PHYSICS IN MEDICINE AND BIOLOGY

Phys. Med. Biol. **58** (2013) 169–182 doi:10.1088/0031-9155/58/1/169

Monte Carlo-based evaluation of S-values in mouse models for positron-emitting radionuclides

Tianwu Xie[1] **and Habib Zaidi**[1,2,3,4]

[1] Division of Nuclear Medicine and Molecular Imaging, Geneva University Hospital, CH-1211 Geneva 4, Switzerland
[2] Geneva Neuroscience Center, Geneva University, CH-1205 Geneva, Switzerland
[3] Department of Nuclear Medicine and Molecular Imaging, University Medical Center Groningen, University of Groningen, 9700 RB Groningen, The Netherlands

E-mail: habib.zaidi@hcuge.ch

Received 17 September 2012, in final form 5 November 2012
Published 10 December 2012
Online at stacks.iop.org/PMB/58/169

Abstract

In addition to being a powerful clinical tool, Positron emission tomography (PET) is also used in small laboratory animal research to visualize and track certain molecular processes associated with diseases such as cancer, heart disease and neurological disorders in living small animal models of disease. However, dosimetric characteristics in small animal PET imaging are usually overlooked, though the radiation dose may not be negligible. In this work, we constructed 17 mouse models of different body mass and size based on the realistic four-dimensional MOBY mouse model. Particle (photons, electrons and positrons) transport using the Monte Carlo method was performed to calculate the absorbed fractions and S-values for eight positron-emitting radionuclides (C-11, N-13, O-15, F-18, Cu-64, Ga-68, Y-86 and I-124). Among these radionuclides, O-15 emits positrons with high energy and frequency and produces the highest self-absorbed S-values in each organ, while Y-86 emits γ-rays with high energy and frequency which results in the highest cross-absorbed S-values for non-neighbouring organs. Differences between S-values for self-irradiated organs were between 2% and 3%/g difference in body weight for most organs. For organs irradiating other organs outside the splanchnocoele (i.e. brain, testis and bladder), differences between S-values were lower than 1%/g. These appealing results can be used to assess variations in small animal dosimetry as a function of total-body mass. The generated database of S-values for various radionuclides can be used in the assessment of radiation dose to mice from different radiotracers in small animal PET experiments, thus

[4] Author to whom any correspondence should be addressed.

offering quantitative figures for comparative dosimetry research in small animal models.

S Online supplementary data available from stacks.iop.org/PMB/58/169/mmedia

(Some figures may appear in colour only in the online journal)

1. Introduction

Besides enabling the study of disease in its natural state, *in vivo* small animal imaging assays are used to guide the discovery and development of new treatments of human disease. Mice are widely used in preclinical research studies to develop and test new treatments and imaging methods for human diseases (Hanahan 1989, Tuveson and Hanahan 2011, Deroose *et al* 2007). Radiotracer techniques using positron emission tomography (PET) are commonly used to provide *in vivo* functional imaging noninvasively in small animals, thus enabling us to track molecular processes associated with various diseases (Tai and Laforest 2005, Levin and Zaidi 2007, Rowland and Cherry 2008). PET offers the important advantage that each animal can be studied repeatedly and as such, each animal could serve as its own control in longitudinal studies. In such studies, the animal is administered significant levels of radioactivity that result in radiation doses that can change gene expression, tumour characteristics and in some cases cause lethality (Funk *et al* 2004). Therefore, the dosimetric features of the various radiotracers used in PET require special attention and need to be accurately estimated in laboratory animal experiments.

Funk *et al* (2004) investigated the average whole body dose to mouse and rat from PET imaging using [^{18}F]-fluorodeoxyglucose (FDG)as a probe. Mouse and rat models of different mass were represented by ellipsoids with fixed ratios of the principal axes and used by the MCNP code to calculate absorbed fractions from point sources and uniformly distributed sources. Much more sophisticated computational models corresponding to the anatomy and physiology of laboratory animals, which can be thoroughly coupled to radiation transport computer codes are currently available (Zaidi and Xu 2007). Using Monte Carlo simulations, Taschereau and Chatziioannou (2007) evaluated the absorbed dose distribution in mouse from representative small animal PET imaging procedures using FDG, 3'-deoxy-3'-[^{18}F]-fluorothymidine and [^{18}F]-fluoride ions. Four models were used in this work: a voxelized realization of the whole-mouse MOBY model, a high-resolution bladder model, a high-resolution femur head model and a high-resolution vertebra model. Keenan *et al* (2010) calculated S-values for ^{18}F and several other nuclides in a series of small animal models using GEANT4. However, given the availability of new PET tracers and since more precise and accurate preclinical molecular imaging is becoming feasible, short and long term effects of radiation in diagnostic and therapeutic applications involving the use of small animal models became a concern.

A plethora of novel compounds labelled with various positron-emitting radionuclides are available for assessing tumour metabolism and other biologic and physiologic parameters associated with many diseases. Owing to the small size of mouse organs and since cross-irradiation is a matter of concern in small animal dosimetry (Bitar *et al* 2007, Stabin *et al* 2006), additional work is needed to fully characterize the dosimetric properties of different positron-emitting radionuclides.

In this work, we produced 17 voxel-based mouse models of different body mass and size based on the realistic MOBY four-dimensional whole-body mouse model. Absorbed fractions

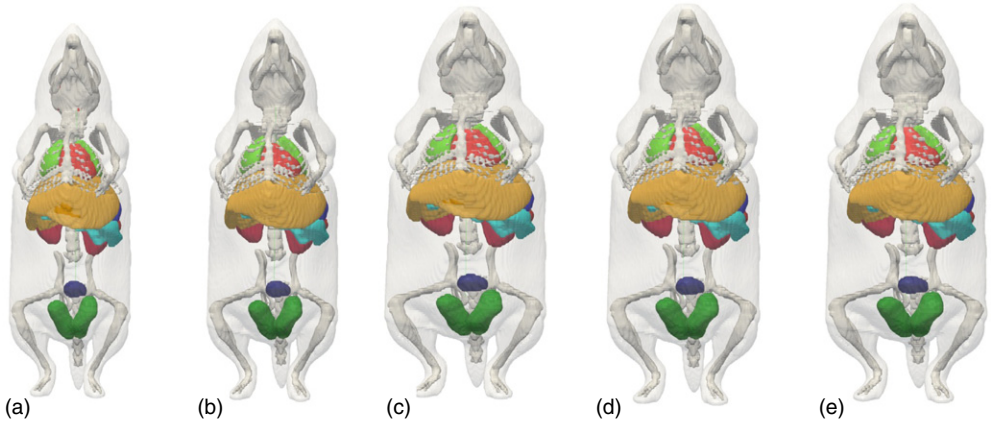

Figure 1. 3D visualization of representative scaled mouse models showing: (a) the 21.09 g, (b) 25.11 g, (c) 27.24 g, (d) 29.81 g and (e) the 35.23 g mouse models.

and S-values were calculated for 22 organs from eight positron-emitting radionuclides (C-11, N-13, O-15, F-18, Cu-64, Ga-68, Y-86 and I-124), which are commonly used to label various probes used in small animal PET imaging (Nanni *et al* 2007, Dence *et al* 2008, Haubner *et al* 2010). In addition, the absorbed dose for some representative radiotracers was assessed using published biodistribution data. Factors affecting the radiation dose associated with small animal PET imaging using different radiotracers are also examined. This work provides detailed radiation dosimetry database that can be used for the assessment of radiation dose to small animals following the administration of various PET probes and provides quantitative figures for comparative dosimetry research using small animal models.

2. Materials and methods

2.1. Scaled mouse models

Using the MOBY software developed by Segars *et al*(2004), we constructed a series of voxel-based mouse models with total body mass ranging between 21 and 35 g. Figure 1 shows the ventral–dorsal views of some scaled mouse models. The dimensions of the mouse models were determined randomly using a normal distribution as described by Kesner *et al* (2006) to represent small animals typically used in preclinical molecular imaging research. The resulting organ and body masses calculated by multiplying each organ volume and its corresponding density are summarized in table 1. The masses of the stomach, small intestine, large intestine and bladder correspond to the sum of wall and contents. The skeleton was treated as a mixture of 70% bone, 25% red bone marrow and 5% yellow bone marrow (Xie *et al* 2010, Schermer 1967).

Seventeen mouse models were generated from the original NURBS-based MOBY model and saved in voxelized format with 200 × 200 × 512 matrix dimension and 0.2 mm cubic voxels. The number of voxels in each organ was calculated and multiplied by the voxel volume and tissue density to yield the organ mass. In the absence of well-established characteristics of small animals, the tissue density and chemical compositions of the mouse model were assumed to be similar to those recommended for humans. This assumption might introduce additional errors of a few percentage points, but are not deemed large enough to

Table 1. Organ densities of small-animal models used in this work.

Organ	Density (g cm^{-3})
Remaining tissues	1.04
Skin	1.1
Heart wall	1.06
Blood in heart	1.06
Liver	1.05
Gall bladder	1.03
Lung	0.3
Stomach	1.04
Pancreas	1.05
Kidney	1.05
Spleen	1.06
Small intestine	1.04
Large intestine	1.04
Bladder	1.04
Vas deferens	1.04
Testis	1.04
Skeleton	1.4
Brain	1.04
Thyroid	1.05

significantly affect absorbed dose calculations (Stabin 2008, Keenan *et al* 2010, Xie *et al* 2012).

2.2 Absorbed dose and S-values

The MIRD schema (Bolch *et al* 2009) for internal dosimetry was used in this work to calculate the mean absorbed dose. In most situations, since the changes of source and target masses can be neglected, the S-values of certain source–target pairs for a specific radionuclide remain constant over the period of irradiation. The mean absorbed dose $D\,(r_T, T_D)$ is given by

$$D(r_T, T_D) = \sum_{r_S} \int_0^{T_D} \tilde{A}(r_S, t) S(r_T \leftarrow r_S)\, \mathrm{d}t, \tag{1}$$

where $\tilde{A}(r_S, t)$ is the cumulated (time-integrated) activity in source tissue r_S over dose-integration period T_D:

$$\tilde{A}(r_S, T_D) = \int_0^{T_D} A(r_S, t)\, \mathrm{d}t, \tag{2}$$

$S(r_T \leftarrow r_S)$ is the S-value describing the equivalent dose rate in the target organ per unit activity in the source organ:

$$S(r_T \leftarrow r_S) = \frac{1}{M(r_T)} \sum_i E_i Y_i \phi(r_T \leftarrow r_S, E_i), \tag{3}$$

where E_i is the individual energy of the ith nuclear transition, Y_i is number of ith nuclear transitions per nuclear transformation, $M(r_T)$ is the mass of the target tissue r_T, and $\phi(r_T \leftarrow r_S, E_i)$ is the absorbed fraction (AF) of radiation energy Ei in the target organ for the ith radiation type originating in the source organ. The AF describes the proportion of energy released in the source organ deposited in the target organ.

2.3. Monte Carlo simulations

MCNP is a powerful general-purpose Monte Carlo code for simulating photon, neutron, electron and coupled neutron/photon/electron transport and is now widely used in radiation dosimetry (Xu and Eckerman 2009). The MCNPX version (Waters *et al* 2007), MCPLIB02 photon cross section library and default electron/positron transport algorithms were adopted in this work for radiation transport simulations. Uniformly distributed photon, positron and electron sources were simulated in 19 chosen source regions. The energy deposited from photons, electrons and positrons originating in the target regions were recorded using MCNPX tally card *F8 and used to derive S-values according to equation (4). A total of 6.0×10^6 primary particle histories (NPS) were generated, and the statistical uncertainty in terms of coefficient of variation (COV) was less than 2% in most cases. The S-values for each particle type emitted were aggregated as the S-values for a given radionuclide. The decay data of the eight positron-emitting radionuclides (C-11, N-13, O-15, F-18, Cu-64, Ga-68, Y-86 and I-124) investigated in this work were acquired from the Health Physics Society electronic resource (HPS 2012).

3. Results

The organ mass and body size of the seventeen mouse models are summarized in table 2. Organ S-values for the eight radionuclides for mouse models of various size and mass were calculated. Supplemental tables I–IV (available from stacks.iop.org/PMB/58/169/mmedia), provide the calculated S-values corresponding to the eight positron-emitting radionuclides (C-11, N-13, O-15, F-18, Cu-64, Ga-68, Y-86 and I-124) for 21, 25, 30 and 35 g mouse models, respectively. Figure 2 shows the self-absorbed S-values for the selected positron-emitting radionuclides for 19 target organs of the 17 mouse models. For most organs, the largest self-absorbed S-values are obtained for O-15, whereas the smallest self-absorbed S-values are found for I-124. Figures 2(a) and (b) shows that self-absorbed organ S-values from F-18 are about 50% smaller than from O-15. Figure 2(c) demonstrates that for radionuclides (C-11, N-13, O-15, F-18 and Ga-68) that emit more than 75% of positrons during their decay, differences between S-values are less than 15% indicating that the low density of lung, small mass of thyroid and gall bladder, narrow geometry of vas deferens, skin and heart wall may facilitate the escape of particles, thus resulting in similar self-absorbed S-values.

Figures 3 and 4 show representative self-absorbed S-values and cross-absorbed S-values, respectively, for selected organs as a function of body mass for the selected positron-emitting radionuclides. S-value curves follow a gradual reduction when the body mass increases. Oxygen-15 presents the largest self-absorbed S-values (figure 3) in source organs because of the high-energy (0.735 MeV) and large amount of positrons emitted from its nuclear transformation. The largest cross-absorbed S-values for adjacent target organs and non-adjacent target organs were obtained for Ga-68 and Y-86, respectively. The smallest cross-absorbed S-values were obtained for Cu-64.

Based on the obtained results, we evaluated the body weight-based percentage differences of S-values for F-18, Y-86 and I-124 for selected organ pairs from 21 to 35 g mouse models (table 3). Meanwhile, to verify the calculation of S-values using MCNPX, we modified the original MOBY model to match the 30 g mouse model reported by Keenan *et al* (2010) and compared the self-absorbed S-values for ^{18}F between these two works (table 4). Overall, there is good agreement between the estimated ^{18}F S-values in our work and those reported by Keenan *et al* (2010).

Table 2. Summary of organ masses and body sizes for the 17 scaled anatomical mouse models.

		Scaled mouse models																		
		1	2	3	4	5	6	7	8	9	10	11	12	13	14	15	16	17	Mean	SD
Mass (g)	Remaining Tissues	13.45	14.06	14.10	15.70	16.14	16.16	17.30	17.61	18.21	18.30	19.05	19.31	19.89	20.15	20.44	20.93	23.01	17.87	2.68
	Skin	1.64	1.67	1.67	1.72	1.71	1.77	1.77	1.82	1.85	1.83	1.88	1.94	1.95	2.02	1.96	1.98	2.08	1.84	0.13
	Heart wall	0.05	0.05	0.05	0.06	0.06	0.06	0.06	0.06	0.07	0.07	0.07	0.07	0.07	0.07	0.07	0.08	0.08	0.06	0.01
	Blood in heart	0.16	0.17	0.17	0.18	0.19	0.19	0.20	0.20	0.21	0.21	0.22	0.22	0.23	0.23	0.24	0.24	0.26	0.21	0.03
	Liver	1.19	1.25	1.25	1.40	1.44	1.44	1.55	1.57	1.63	1.64	1.71	1.73	1.78	1.81	1.83	1.88	2.07	1.60	0.25
	Gall bladder	0.01	0.01	0.01	0.01	0.01	0.01	0.01	0.01	0.01	0.01	0.01	0.01	0.01	0.01	0.01	0.01	0.01	0.01	0.00
	Lung	0.11	0.12	0.12	0.13	0.13	0.13	0.14	0.15	0.15	0.15	0.16	0.16	0.16	0.17	0.17	0.18	0.19	0.15	0.02
	Stomach	0.33	0.35	0.35	0.39	0.40	0.40	0.43	0.44	0.45	0.45	0.47	0.48	0.49	0.50	0.51	0.52	0.57	0.44	0.07
	Pancreas	0.23	0.25	0.25	0.27	0.28	0.28	0.30	0.31	0.32	0.32	0.33	0.34	0.35	0.35	0.36	0.37	0.40	0.31	0.05
	Kidney	0.22	0.23	0.23	0.25	0.26	0.26	0.28	0.29	0.29	0.30	0.31	0.31	0.32	0.33	0.33	0.34	0.37	0.29	0.04
	Spleen	0.07	0.07	0.07	0.08	0.08	0.08	0.09	0.09	0.09	0.09	0.10	0.10	0.10	0.10	0.10	0.11	0.12	0.09	0.01
	Small intestine	1.13	1.19	1.19	1.32	1.36	1.36	1.45	1.48	1.53	1.54	1.60	1.62	1.67	1.69	1.72	1.76	1.93	1.50	0.22
	Large intestine	0.39	0.40	0.40	0.45	0.46	0.46	0.50	0.50	0.52	0.52	0.54	0.55	0.57	0.58	0.58	0.60	0.66	0.51	0.08
	Bladder	0.04	0.04	0.04	0.05	0.05	0.05	0.05	0.06	0.06	0.06	0.06	0.06	0.06	0.06	0.06	0.07	0.07	0.06	0.01
	Vas deferens	0.02	0.02	0.02	0.02	0.02	0.02	0.02	0.02	0.02	0.02	0.02	0.02	0.02	0.02	0.02	0.02	0.02	0.02	0.00
	Testis	0.21	0.22	0.22	0.25	0.25	0.25	0.27	0.27	0.28	0.29	0.30	0.30	0.31	0.31	0.32	0.33	0.36	0.28	0.04
	Skeleton	1.51	1.57	1.57	1.73	1.77	1.79	1.89	1.92	1.98	1.99	2.07	2.10	2.15	2.18	2.20	2.25	2.45	1.95	0.27
	Brain	0.32	0.34	0.34	0.38	0.39	0.39	0.41	0.42	0.44	0.44	0.46	0.46	0.48	0.48	0.49	0.50	0.55	0.43	0.06
	Thyroid	0.01	0.01	0.01	0.01	0.01	0.01	0.01	0.01	0.01	0.01	0.01	0.01	0.01	0.01	0.01	0.01	0.01	0.01	0.00
	Total body	21.09	22.00	22.06	24.40	25.02	25.11	26.74	27.24	28.13	28.25	29.36	29.81	30.65	31.08	31.44	32.16	35.23	27.63	3.97
Size (mm)	LAT	27.09	27.52	27.44	27.20	26.44	28.33	26.60	29.46	28.60	28.14	28.57	31.92	28.81	34.48	30.00	30.43	33.99	29.12	2.40
	AP	15.15	15.79	15.86	17.94	19.24	17.52	20.62	19.05	19.71	20.43	20.87	19.02	21.09	18.43	21.19	21.49	21.71	19.12	2.09
	Height	89.84	88.98	89.09	88.98	87.91	90.05	87.69	87.27	89.84	88.66	89.09	88.66	91.34	88.45	89.84	89.52	87.48	88.98	1.05

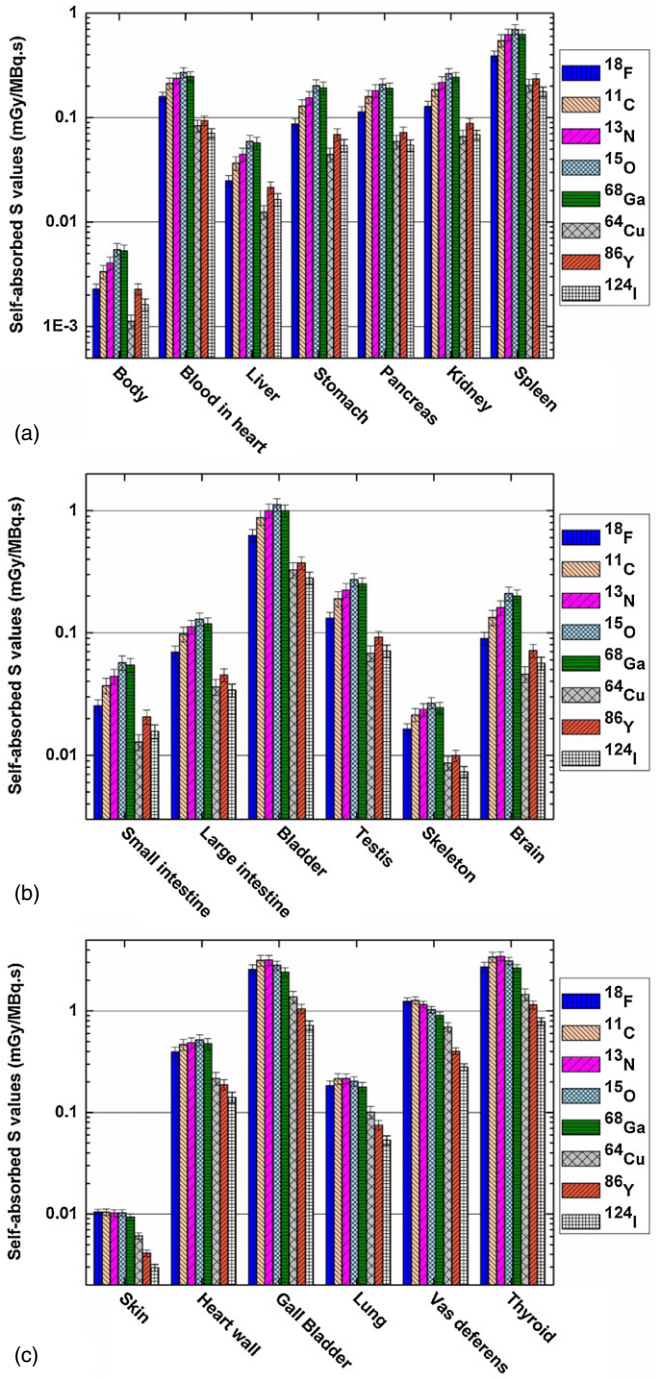

Figure 2. Comparison of self-absorbed S-values for the 17 mouse models for different positron-emitting radionuclides.

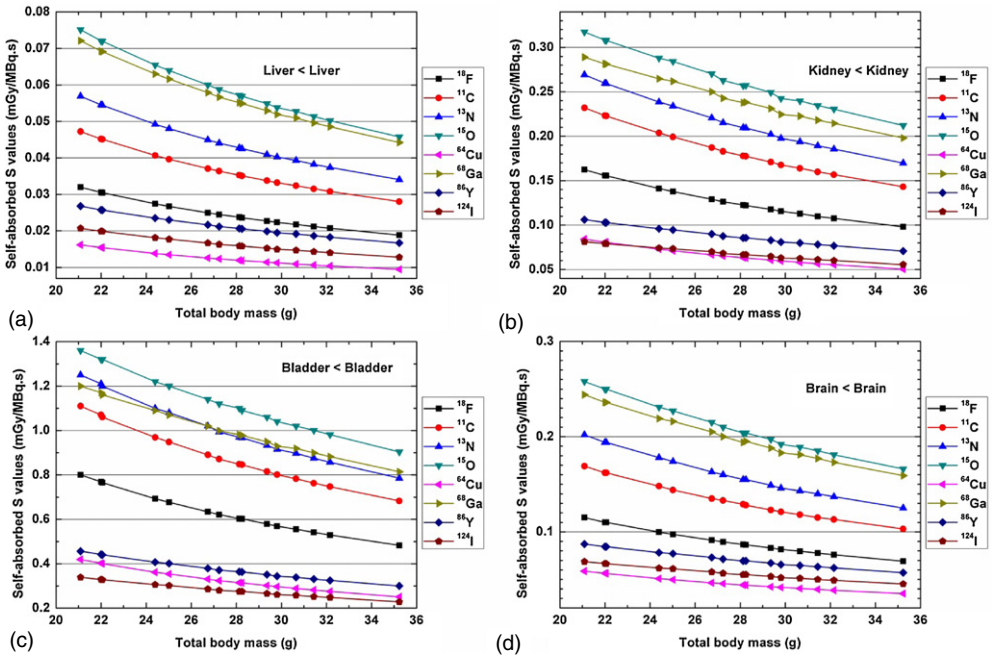

Figure 3. Representative self-absorbed S-values for selected organs as a function of body mass for different positron-emitting radionuclides.

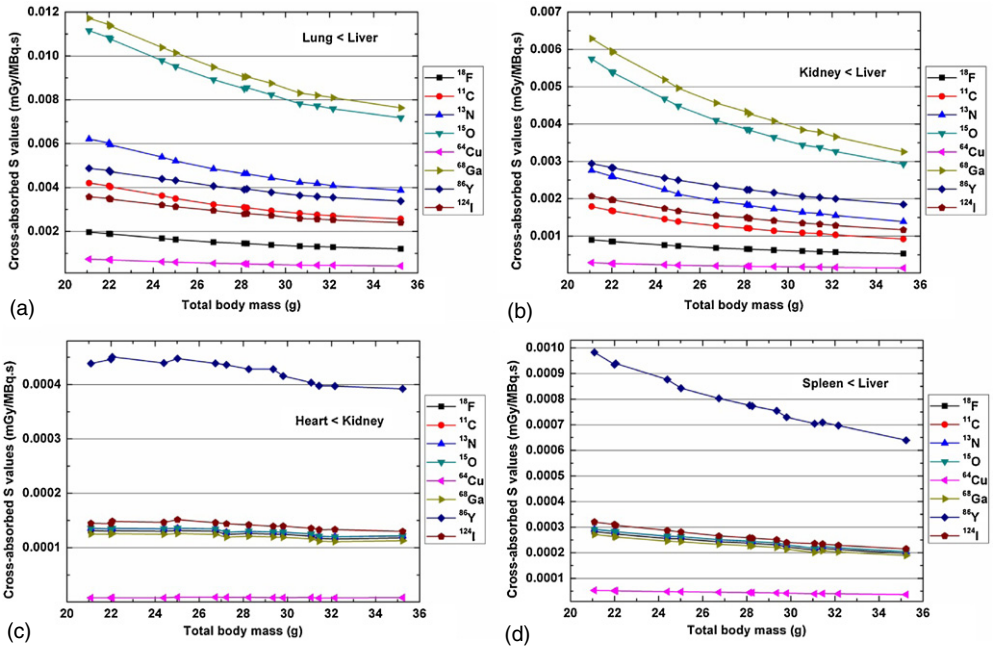

Figure 4. Representative cross-absorbed S-values for selected organs as a function of body mass for different positron-emitting radionuclides.

Table 3. Percentage difference between S-values per gram difference in total body mass for mouse models ranging between 21 and 35 g for ^{18}F, ^{86}Y and ^{124}I.

^{18}F (%/g)							
Organ	Liver	Stomach	Kidney	Spleen	Bladder	Testis	Brain
Liver	−2.90	−2.94	−2.95	−2.31	0.08	0.12	0.03
Stomach	−2.95	−2.88	−1.58	−3.32	−0.28	0.00	0.22
Kidney	−2.92	−1.65	−2.80	−2.34	−1.03	−0.24	0.02
Spleen	−2.13	−3.32	−2.39	−2.72	−0.85	−0.23	0.72
Bladder	−0.25	−0.39	−0.73	−0.87	−2.80	−0.97	−0.76
Testis	0.08	0.14	−0.16	−0.10	−0.90	−2.77	0.66
Brain	0.02	−0.11	0.37	0.41	0.31	0.05	−2.81
^{86}Y (%/g)							
Organ	Liver	Stomach	Kidney	Spleen	Bladder	Testis	Brain
Liver	−2.66	−2.94	−2.62	−2.40	−0.23	0.07	0.12
Stomach	−2.93	−2.61	−2.06	−2.96	−0.07	0.21	0.21
Kidney	−2.63	−2.19	−2.35	−2.56	−1.00	−0.38	−0.13
Spleen	−2.47	−3.00	−2.59	−2.31	−1.03	−1.12	0.04
Bladder	0.50	0.05	−0.46	−1.23	−2.43	−1.50	0.43
Testis	0.24	−0.18	−0.32	−0.63	−1.51	−2.38	0.43
Brain	0.05	−0.01	0.19	0.48	1.39	0.93	−2.43
^{124}I (%/g)							
Organ	Liver	Stomach	Kidney	Spleen	Bladder	Testis	Brain
Liver	−2.70	−3.35	−3.04	−2.33	−0.16	0.13	0.08
Stomach	−3.32	−2.62	−2.81	−3.24	−0.12	0.37	−0.24
Kidney	−3.08	−2.87	−2.24	−3.11	−1.02	−0.25	0.64
Spleen	−2.32	−3.26	−3.16	−2.19	−1.08	−0.72	0.60
Bladder	0.20	−0.39	−0.64	−0.37	−2.31	−2.09	0.48
Testis	0.26	−0.20	−0.13	−0.24	−2.08	−2.29	0.72
Brain	−0.01	0.26	0.38	0.51	0.66	0.78	−2.42

Table 4. Comparison of self-absorbed S-values (mGy/MBq-s) from ^{18}F in a 30g MOBY mouse model calculated in this work and those reported by Keenan *et al* (2010).

	This work	Keenan *et al*
Bladder	4.56E-01	4.59E-01
Brain	6.54E-02	6.71E-02
Heart	1.27E-01	1.27E-01
Kidneys	9.45E-02	9.68E-02
Liver	1.84E-02	1.82E-02
Pancreas	9.10E-02	9.15E-02
Skeleton	1.26E-02	1.23E-02
Spleen	2.51E-01	2.56E-01
Testes	1.80E-01	1.81E-01
Thyroid	1.88E+00	1.93E+00

The contribution from different types of radiation to the S-values of positron-emitting radionuclides is shown in figure 5. For C-11, N-13, O-15, F-18 and Ga-68, over 92% of the total self-absorbed S-values originate from positrons. For F-18 and Y-86, more than half of the total cross-absorbed S-values arise from photons and x-rays. For Cu-64, the contribution of positrons to the total S-value is lower than 40%.

To extend further the assessment to absorbed dose in small animals following the administration of positron-emitting tracers, we selected a few preclinical studies as examples

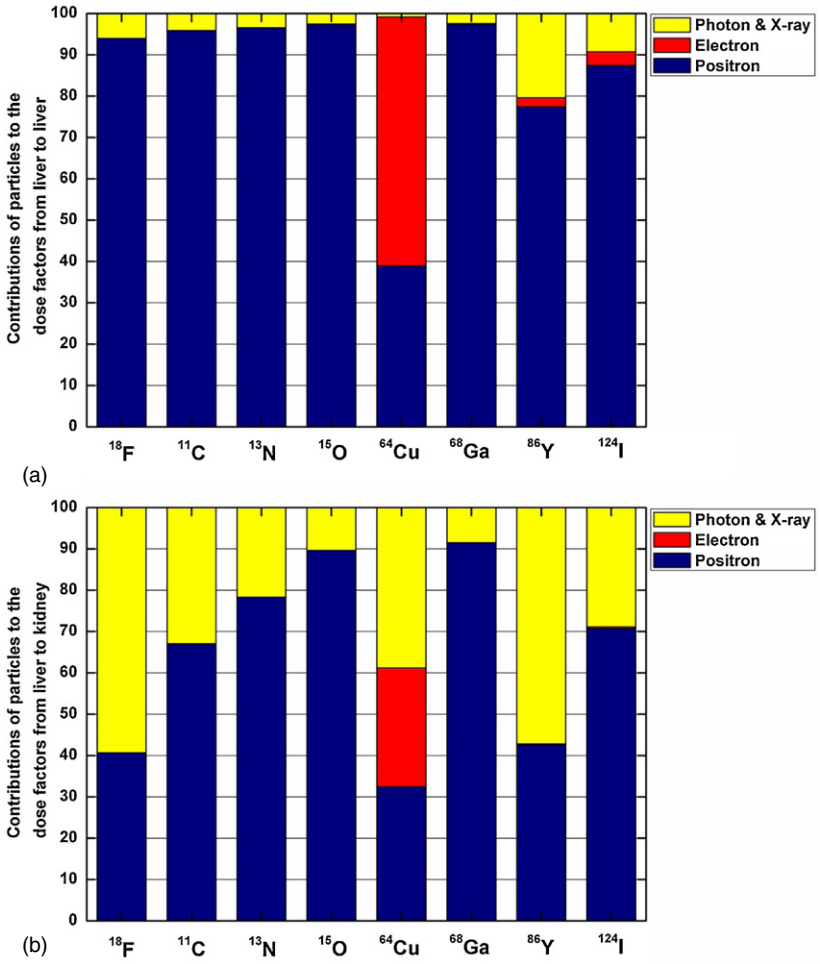

Figure 5. Relative contributions of different types of radiation (photons and x-rays, electrons and positrons) to the estimated S-values.

and performed absorbed dose calculations using published mouse biodistribution data and S-values derived from our calculations. For example, Silva (2010) used dynamic whole body PET studies to evaluate FDG distribution in the mouse and obtained time activity curves (TACs) at 18 time points from 0 to 90 min. By adopting the atlas-guided PET data analysis method (Gutierrez and Zaidi 2012), we extracted the FDG uptake in 18 source regions at each time point. Within the considered timeframe, TACs were generated using piecewise linear interpolation. No biological washout was assumed and only radionuclide decay was considered to affect the activity concentration of the tracers. According to equations (5) and (6), the calculated activities in selected source regions are integrated with time from 0 to ∞ and multiplied by the S-values to obtain the absorbed dose to organs. Table 5 compares the normalized absorbed doses for selected organs/structures of mouse models used in this work and those reported by Taschereau and Chatziioannou (2007). The discrepancies between the absorbed doses in both studies can be mainly attributed to the different PET data analysis methods and the characteristics and resulting large variations in terms of FDG biodistributions in the two mouse specimens used. Moreover, the differences between this and Taschereau's

Table 5. Comparison of calculated absorbed doses from FDG in selected organs/structures of the MOBY phantom between this work and those reported by Taschereau and Chatziioannou (2007). The absorbed doses for the 17 mouse models (21–35 g) are also shown. The tabulated absorbed doses are normalized per MBq administered activity.

Organs	This work (MOBY) (mGy/MBq)	Taschereau *et al* (mGy/MBq)	This work (17 models) (mGy/MBq)
Skin	1.91	2.57	2.28 ± 0.30
Liver	10.23	5.68	13.72 ± 2.06
Lung	38.67	9.05	48.99 ± 7.24
Stomach	7.06	4.32	8.96 ± 1.29
Pancreas	11.64	13.51	14.35 ± 2.12
Kidney	25.64	26.35	34.42 ± 5.04
Spleen	9.65	12.97	14.20 ± 2.00
Small intestine	8.92	–	12.20 ± 1.75
Large intestine	11.21	–	15.34 ± 2.20
Bladder	144.56	529.05	198.10 ± 29.00
Vas deferens	20.16	29.86	25.27 ± 3.40
Testis	22.45	15.95	16.82 ± 2.41
Skeleton	5.38	4.86	6.52 ± 0.91
Brain	2.30	13.24	2.58 ± 0.34
Thyroid	7.87	14.19	10.36 ± 1.38

results can be mainly attributed to the different PET data analysis methods and the different FDG biodistributions between the two mouse specimens used. The brain region was missing in the FDG-PET study used in this work and as such, the absorbed dose for the brain in our work refers to the cross-absorbed dose only, which resulted in significantly lower values compared to results reported by Taschereau and Chatziioannou (2007).

In addition, we selected from the literature a number of ^{11}C-labelled tracers used in small-animal PET imaging to assess the corresponding absorbed dose to the 17 mouse models. This includes a ^{11}C-labelled analogue of a potent tyrosine-based peroxisome proliferator–activated receptor agonist (^{11}C-GW7845), which is an inhibitor of experimental mammary carcinogenesis (Mathews *et al* 2005), 5–^{11}C-methyl-3-(2-(S)-azetidinylmethoxy)pyridine (^{11}C-5MA) as PET imaging agent for brain nicotinic acetylcholine receptors on mouse (Iida *et al* 2004), N-benzyl-N-ethyl-2-(7-^{11}C-methyl-8-oxo-2-phenyl-7,8-dihydro-9H-purin-9-yl)acetamide ^{11}C-AC5216) as a PET ligand for imaging of the peripheral benzodiazepine receptor (Yamasaki *et al* 2011) and ^{11}C-labelled topotecan (^{11}C-TPT) as a new probe in small animal PET imaging (Zhang *et al* 2007). Published biodistribution data were used to calculate the absorbed dose for these four ^{11}C-labelled radiotracers in mouse models of different mass. The results are shown in figure 6.

4. Discussion

Current and future generation PET molecular imaging probes, assays and imaging systems still have substantial room for improvement in order to improve PET's ability to detect, visualize and quantify low concentrations of probes interacting with its target, which is referred to as the *molecular sensitivity* (Levin and Zaidi 2007), in order to accurately study the subtle signatures associated with these molecular processes. The molecular sensitivity is defined by a combination of the probe and biological/physiological properties of the subject that define its differential concentration in the cellular and molecular targets of disease states, and the performance capabilities of the imaging system that determine the accuracy and precision to which the resulting signal may be measured. Novel imaging system technology advances,

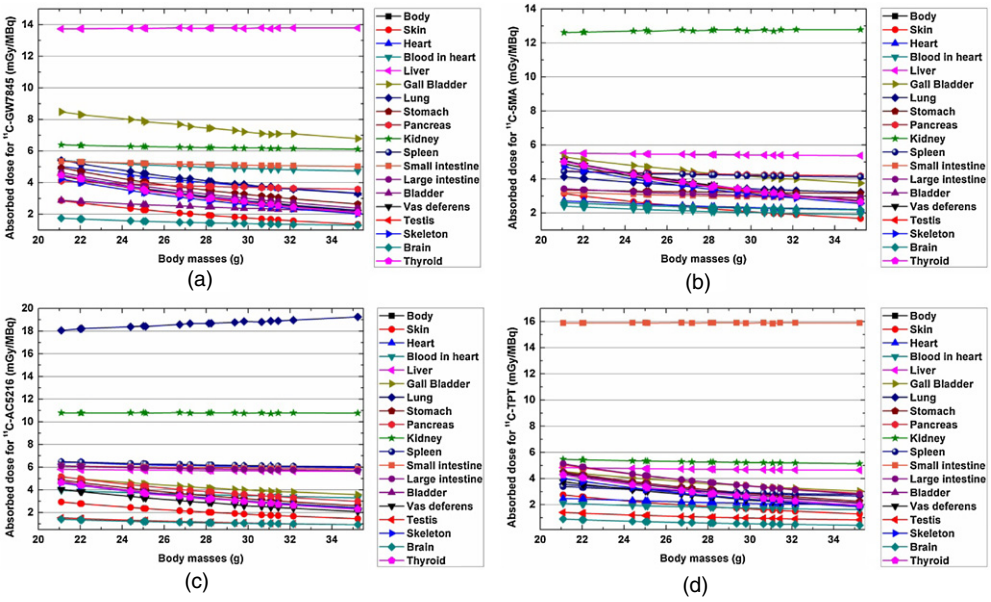

Figure 6. Absorbed doses for internal organs of the 17 mouse models resulting from four representative ^{11}C-labelled radiotracers used in small animal PET imaging: (a) ^{11}C-GW7845; (b) ^{11}C-5MA; (c) ^{11}C-AC5216; (d) ^{11}C-TPT.

together with new probe molecules that target specific molecular processes associated with disease, will undeniably continue to increase PET's role in the study of disease and development of novel treatments.

In this work, we calculated S-values for eight positron-emitting radionuclides that can be used to estimate the internal organ dose for mouse in small animal PET imaging experiments. O-15, Ga-68 and Y-86 present the largest S-values in source organs, adjacent target organs and non-adjacent target organs, respectively. Cu-64 presents significantly lower absorbed S-values compared to other radionuclides in most organs, especially in non-adjacent target organs. The results show that the S-values of positron-emitting radionuclides for different organs correlate very strongly with the source-target distance and the decay scheme of the radionuclide. Radionuclides of high energy and large amount of emitted positrons (e.g. O-15 and Ga-68) are more likely to deliver a very high local dose inside and around the source organ, while the whole body absorbed dose remains low.

The variations of organ S-values with changes in total body mass were also investigated. Overall, S-values decrease with an increase in total body mass because the organ masses are larger. This difference is more important than the small increases in absorbed fractions that occur because of higher particle deposited energy in organs. Differences in S-values for organs self-irradiation are between 2.2% and 3.0% per gram of difference in body weight for the investigated radionuclides. For organs irradiating other organs outside the splanchnocoele (i.e. brain, testis and bladder), most differences of cross-absorbed S-values are lower than 1%/g and as such, are not perceptible within the uncertainties of the calculations. These organs may thus be less relevant than organs inside the splanchnocoele when looking at differences in absorbed doses resulting from changes in body mass.

Based on the calculated S-values and biodistribution data gathered from small animal PET studies, we evaluated the absorbed dose to mouse models from various radiotracers. As can be seen in table 5, the absorbed dose depends on the time-related biodistribution of FDG,

which can vary for different organs and specimens. The mouse studies used in this work and by Taschereau correspond to a normal adult mouse and a tumour bearing mouse, respectively. The different FDG biodistributions between the two specimens results in substantial variations of absorbed dose distributions.

For using the same radionuclide (C-11), the absorbed dose to organs resulting from the administration of different radiotracers depends strongly on the biological half-lives and biodistribution data. The highest absorbed doses from ^{11}C-GW7845, ^{11}C-5MA, ^{11}C-AC5216 and ^{11}C-TPT are observed in the liver, kidney, lung and small intestine, in which the radiotracers have a high uptake level and long residence time, respectively. For organs receiving most of their radiation dose from cross irradiations, the normalized absorbed dose decreases with increasing the body mass because of the larger organ mass and larger organ separation.

5. Conclusion

We reported S-values for various mouse models from eight positron-emitting radionuclides used in small animal PET imaging and evaluated the variation of S-values with changes in body mass. Among the eight radionuclides, O-15 produces the highest S-values in source organs, while Ga-68 produces the highest cross-absorbed S-values in adjacent target organs and Y-86 produces the highest cross-absorbed S-values in non-adjacent target organs. The S-values for internal organs from different radionuclides correlate strongly with the anatomic properties of the organs and nuclear decay schemes and energy spectra of the radionuclides. Variations of self-absorbed S-values for all studied radionuclides are in the range 2.2–3.0%/g difference in body weight. For organs irradiating other organs outside the splanchnocoele (i.e. brain, testis and bladder), differences in S-values are not perceptible within the uncertainties of the data.

These differences are appealing and can be used to evaluate variations in small animal dosimetry as a function of total body mass. The calculated S-values for radionuclides can also be used in the assessment of radiation dose from different radiotracers to mice in small animal PET imaging. For different radiotracers labelled by the same radionuclide, the resulting dose distributions depend on the time-related biodistributions and present significant discrepancies.

Acknowledgments

This work was supported by the Swiss National Science Foundation under grant SNSF 31003A-125246, Geneva Cancer League and the Indo-Swiss Joint Research Programme ISJRP 138866.

References

Bitar A, Lisbona A, Thedrez P, Sai Maurel C, Le Forestier D, Barbet J and Bardies M 2007 A voxel-based mouse for internal dose calculations using Monte Carlo simulations (MCNP) *Phys. Med. Biol.* **52** 1013–25

Bolch W E, Eckerman K F, Sgouros G and Thomas S R 2009 MIRD Pamphlet No. 21: a generalized schema for radiopharmaceutical dosimetry-standardization of nomenclature *J. Nucl. Med.* **50** 477–84

Dence C S, Ponde D E, Welch M J and Lewis J S 2008 Autoradiographic and small-animal PET comparisons between 18F-FMISO, 18F-FDG, 18F-FLT and the hypoxic selective 64Cu-ATSM in a rodent model of cancer *Nucl. Med. Biol.* **35** 713–20

Deroose C M, De A, Loening A M, Chow P L, Ray P, Chatziioannou A F and Gambhir S S 2007 Multimodality imaging of tumor xenografts and metastases in mice with combined small-animal PET, small-animal CT, and bioluminescence imaging *J. Nucl. Med.* **48** 295–303 (available at http://jnm.snmjournals.org/content/48/2/295.short)

Funk T, Sun M and Hasegawa B H 2004 Radiation dose estimate in small animal SPECT and PET *Med. Phys.* **31** 2680–6

Gutierrez D and Zaidi H 2012 Automated analysis of small animal PET studies through deformable registration to an Atlas *Eur. J. Nucl. Med. Mol. Imaging* **39** 1807–20

Hanahan D 1989 Transgenic mice as probes into complex systems *Science* **246** 1265–75

Haubner R, Beer A J, Wang H and Chen X 2010 Positron emission tomography tracers for imaging angiogenesis *Eur. J. Nucl. Med. Mol. Imaging* **37** 86–103

Health Physics Society (HPS) 2012 http://hps.org/publicinformation/radardecaydata.cfm

Iida Y, Ogawa M, Ueda M, Tominaga A, Kawashima H, Magata Y, Nishiyama S, Tsukada H, Mukai T and Saji H 2004 Evaluation of 5-11C-methyl-A-85380 as an imaging agent for PET investigations of brain nicotinic acetylcholine receptors *J. Nucl. Med.* **45** 878–84 (available at http://jnm.snmjournals.org/content/45/5/878.short)

Keenan M A, Stabin M G, Segars W P and Fernald M J 2010 RADAR realistic animal model series for dose assessment *J. Nucl. Med.* **51** 471–6

Kesner A L, Dahlbom M, Huang S C, Hsueh W A, Pio B S, Czernin J, Kreissl M, Wu H M and Silverman D H 2006 Semiautomated analysis of small-animal PET data *J. Nucl. Med.* **47** 1181–6 (available at http://jnm.snmjournals.org/content/47/7/1181.short)

Levin C S and Zaidi H 2007 Current trends in preclinical PET system design *PET Clin.* **2** 125–60

Mathews W B, Foss C A, Stoermer D, Ravert H T, Dannals R F, Henke B R and Pomper M G 2005 Synthesis and biodistribution of 11C-GW7845, a positron-emitting agonist for peroxisome proliferator–activated receptor-γ *J. Nucl. Med.* **46** 1719–26 (available at http://jnm.snmjournals.org/content/46/10/1719.short)

Nanni C, Rubello D and Fanti S 2007 Role of small animal PET for molecular imaging in pre-clinical studies *Eur. J. Nucl. Med. Mol. Imaging* **34** 1819–22

Rowland D J and Cherry S R 2008 Small-animal preclinical nuclear medicine instrumentation and methodology *Sem. Nucl. Med.* **38** 209–22

Schermer S 1967 *The Blood Morphology of Laboratory Animals* (Philadelphia, PA: Davis)

Segars W P, Tsui B M W, Frey E C, Johnson G A and Berr S S 2004 Development of a 4-D digital mouse phantom for molecular imaging research *Mol. Imaging Biol.* **6** 149–59

Silva S E O B 2010 Small animal PET imaging using GATE Monte Carlo simulations: implementation of physiological and metabolic information *PhD Thesis* Faculdade de Ciências,Universidade de Lisboa, Lisboa

Stabin M G 2008 Uncertainties in internal dose calculations for radiopharmaceuticals *J. Nucl. Med.* **49** 853–60

Stabin M G, Peterson T E, Holburn G E and Emmons M A 2006 Voxel-based mouse and rat models for internal dose calculations *J. Nucl. Med.* **47** 655–9 (available at http://jnm.snmjournals.org/content/47/4/655.short)

Tai Y C and Laforest R 2005 Instrumentation aspects of animal PET *Annu. Rev. Biomed. Eng.* **7** 255–85

Taschereau R and Chatziioannou A F 2007 Monte Carlo simulations of absorbed dose in a mouse phantom from 18-fluorine compounds *Med. Phys.* **34** 1026–36

Tuveson D and Hanahan D 2011 Translational medicine: cancer lessons from mice to humans *Nature* **471** 316–7

Waters L S, McKinney G W, Durkee J W, Fensin M L, Hendricks J S, James M R, Johns R C and Pelowitz D B 2007 The MCNPX Monte Carlo radiation transport code *Hadronic Shower Simulation Workshop (AIP Conf. Proc.)* vol 896 pp 81–90

Xie T, Han D, Liu Y, Sun J and Liu Q 2010 Skeletal dosimetry in a voxel-based rat phantom for internal exposures to photons and electrons *Med. Phys.* **37** 2167–78

Xie T, Liu Q and Zaidi H 2012 Evaluation of S-values and dose distributions for 90Y, 131I, 166Ho, and 188Re in seven lobes of the rat liver *Med. Phys.* **39** 1462–72

Xu X G and Eckerman K F eds 2009 *Handbook of Anatomical Models for Radiation Dosimetry* (London: Taylor and Francis)

Yamasaki T *et al* 2011 Evaluation of the P-glycoprotein- and breast cancer resistance protein-mediated brain penetration of 11C-labeled topotecan using small-animal positron emission tomography *Nucl. Med. Biol.* **38** 707–14

Zaidi H and Xu X G 2007 Computational anthropomorphic models of the human anatomy: The path to realistic Monte Carlo modeling in medical imaging *Annu. Rev. Biomed. Eng.* **9** 471–500

Zhang M R, Kumata K, Maeda J, Yanamoto K, Hatori A, Okada M, Higuchi M, Obayashi S, Suhara T and Suzuki K 2007 11C-AC-5216: a novel PET ligand for peripheral benzodiazepine receptors in the primate brain *J. Nucl. Med.* **48** 1853–61